Adsorption of iron(III), cobalt(II), and nickel(II) on activated carbon derived from *Xanthoceras Sorbifolia* Bunge hull: mechanisms, kinetics and influencing parameters

Xiaotao Zhang, Yinan Hao, Ximing Wang and Zhangjing Chen

ABSTRACT

Xanthoceras Sorbifolia Bunge hull activated carbon (XSA) was prepared and characterized by Brunauer–Emmett–Teller analysis, scanning electron microscopy and energy dispersive X-ray (EDX) spectroscopy. The ability of XSA as an adsorbent was investigated for the removal of the iron group ions Fe(III), Co(II), and Ni(II) from aqueous solution. Optimum adsorption parameters were determined based on the initial concentrations of the iron group ions, pH, adsorption temperature, and adsorption time in adsorption studies. The maximum monolayer adsorption capacities were 241.13 mg/g for Fe(III), 126.05 mg/g for Co(II), and 187.96 mg/g for Ni(II), respectively. Adsorption kinetics and isotherms showed that the adsorption process best fitted the nonlinear pseudo-second-order and Langmuir models, and the affinity of the ions for XSA decreased as follows: Fe(III) > Ni(II) > Co(II). Regeneration studies indicated that XSA could be used after several consecutive adsorption/desorption cycles using HNO_3. Fourier transform infrared and EDX spectra revealed the chemical adsorption value of XSA as an adsorbent for removing iron group ions from aqueous solutions.

Key words | activated carbon, adsorption, Fe(III), Co(II), Ni(II), *Xanthoceras sorbifolia* Bunge hull

Xiaotao Zhang
College of Science, Inner Mongolia Agricultural University,
Hohhot 010018,
China

Xiaotao Zhang
Yinan Hao
Ximing Wang (corresponding author)
College of Material Science and Art Design, Inner Mongolia Agricultural University,
Hohhot 010018,
China
E-mail: *w_ximing@263.net*

Zhangjing Chen
Department of Sustainable Biomaterials, Virginia Tech University,
Blacksburg,
VA 24061,
USA

INTRODUCTION

Rapid development of industrialization and urbanization processes can generate large amounts of toxic heavy metal ions that can contaminate surface and groundwater resources. Once heavy metals have been released into natural and man-made ecosystems, even at trace levels, the ions do not biodegrade and may bioaccumulate in living tissues through the food chain, resulting in the uptake of heavy metals by humans and other organisms, impacting human health and inhibiting the growth of aquatic organisms (Tabrizi & Zamani 2016). Thus, the removal of heavy metals from industrial pollution has become a critical and global environmental problem. Heavy metal pollution results from Fe(III), Co(II), and Ni(II) used in mining operations, battery manufacturing, iron and steel industrial units, etc., which are responsible for direct and indirect discharge of effluents into headstreams (Güzel *et al.* 2008).

Many conventional technologies, such as flocculation, membrane separation, ion exchange, adsorption, and hybrid methods combining these techniques have been applied (Tao *et al.* 2015; Dotto *et al.* 2016). Among these approaches, adsorption is one of the most promising technologies because of its high efficiency, low maintenance costs, simplicity to operate and lack of secondary sludge production. Recently, the application of carbonaceous materials as adsorbents for removing heavy metals from wastewater has become an attractive field for scientific studies. Activated carbon is considered as an eco-friendly and effective adsorbent due to its distinctive structure, high surface area, well-developed pore volume and large number of active sites for adsorbing heavy metal ions (Choi *et al.* 2015). Considering economic capital, it is important to produce an abundance of effective activated carbon from low-cost and renewable by-products and agricultural wastes, e.g., watermelon shells, coconut shells, palm shells, walnut shells and other agricultural residues, to serve as adsorbent materials for removing heavy metals from effluents (Daud & Ali 2004; Azevedo *et al.* 2007; Depci *et al.* 2012; Moreno-Barbosa *et al.* 2013).

In the northern region of China, *Xanthoceras sorbifolia* Bunge hull (XSBH) was used to produce activated carbon

doi: 10.2166/wst.2017.067

with extensive reserves but has rarely been used as a precursor for activated carbon for the following two reasons: XSBH may be useful for agricultural waste assessment and to increase the competitiveness of the carbonaceous markets in China. Activated carbon is prepared using physical or chemical activation. In comparison to physical activation, chemical activation is a procedure in which the precursor is treated with chemical agents and then pyrolysed by heating at temperatures of 450–950 °C under a flow of inert gas (nitrogen or argon). Chemical activation is preferred in most cases because it depends on the biomass precursors and results in higher global yields, larger surface area and less burn-off char, and has lower energy costs with lower operating temperatures relative to physical activation (Tang *et al.* 2016). Additionally, chemical activation can result in certain improvements; for example, chemical activation can generate surface functional activation groups, produce new activation sites and strengthen the mechanical stability of the adsorption layers. Agricultural waste activated carbon materials possess basic functional groups containing oxygen, e.g., hydroxyl, carbonyl, phenolic, and alcoholic groups. The various functional groups on the surface of activated carbon have affinities and adsorption capacities for heavy metal ions because they can donate an electron pair to form metal-binding chelates or complexes. The adsorption mechanisms are related to, for example, surface complexation, diffusion through micropores, chemisorption, ion exchange, and electrostatic interactions, which may act alone or together (Oliveira *et al.* 2014). Hence, the potential usage of XSBH as an economic, abundant, renewable, and simple adsorbent for the removal of heavy metal ions from aqueous environments is thoroughly discussed in this paper.

In this work, we successfully produced activated carbon (hereafter termed XSA) from XSBH by using chemical activation with H_3PO_4, and characterized the produced XSA using nitrogen adsorption/desorption isotherms (Brunauer–Emmett–Teller (BET) equation) and scanning electron microscopy/energy dispersive X-ray spectroscopy (SEM/EDX). The prepared XSA was used to remove heavy metal ions, including Fe(III), Co(II), and Ni(II), from aqueous solutions. To date, only a few studies have been reported that compare Fe(III), Co(II), and Ni(II) heavy metal ions. The main novelty of this work is that it can be used to analyse the different adsorption capacities of XSA for the iron group ions Fe(III), Co(II), and Ni(II), which are all located in the fourth period and in group VIII of the periodic table but have different ionic radii, oxidation numbers, electronegativities and valence-electron arrangements. Many factors that influence the adsorption and desorption capacities of Fe(III), Co(II), and Ni(II) by XSA, such as the initial metal concentration, pH, adsorption temperature, adsorption time, desorption agent HNO_3 concentration, desorption temperature and sonicated desorption time, were investigated systematically. Kinetic models were obtained by fitting the experimental data to pseudo-first order, pseudo-second order, intraparticle and Elovich kinetic models, and the equilibrium isotherms were determined using the Langmuir, Freundlich, Temkin, and Dubinin–Radushkevich models. Moreover, the current research presents an exhaustive regeneration study. Finally, we addressed the adsorption mechanisms by using Fourier transform infrared spectroscopy (FTIR). The use of XSA as a low-cost and easily available adsorbent for removing Fe(III), Co(II), and Ni(II) can serve as a valuable reference for controlling the environmental pollution of water.

METHODS

Materials

XSBH was collected from solid waste markets located in Chifeng (China) as a precursor for preparing the activated carbon. Stock solutions of Fe(III), Co(II), and Ni(II) were prepared using their respective nitrate and chloride salts ($Fe(NO_3)_3{\cdot}9H_2O$, $Co(NO_3)_2{\cdot}6H_2O$, and $NiCl_2{\cdot}6H_2O$ (analytical grade)), which were purchased (Tianjin Beilian Fine Chemicals Co., Ltd, China) and prepared in deionized distilled water, and appropriate serial concentrations of each metal ion were prepared using the stock solutions for adsorption experiments. All other commercial chemicals were of analytical reagent grade and were used without further purification. All solutions were prepared using re-ionized distilled water.

Preparation of activated carbon

The samples of XSBH were washed thoroughly with tap water twice and then with hot deionized distilled water to remove leftover rinds, colour, and water-soluble impurities. Next, the samples were dried for 24 hours at 80 °C in a hot air oven (DZF-6210, Shanghai, China) and ground to a powder (0.5–0.8 mm). The chemical activation method was used with H_3PO_4 to prepare the activated carbon from XSBH (Molina-Sabio & Rodrigues-Reinoso 2004). Dried XSBH was washed until the pH of the filtrate was near 7 according to a pH meter (PB-10, Sartorius, Germany) and

dried at 100 °C for 24 h to completely remove moisture. The dried mass was mixed well with H_3PO_4 (45 wt %) and magnetically stirred (500 rpm) at 50 °C for 1 h. The chemical ratio was defined as the weight ratio of H_3PO_4 to the precursor. The slurry was heated to a final carbonization temperature of 500 °C in a tube furnace (FSX2-12-15N, Tianjin, China) for 1 h. Samples were cooled to the room temperature under flowing nitrogen and washed sequentially with deionized distilled water until a neutral pH was attained. The products were then vacuum dried in an oven overnight at 120 °C before crushing, grinding, and passing through 200-mesh sieves (Molina-Sabio & Rodrigues-Reinoso 2004). Yields of 34% were attained. Then, the resulting powdered carbon XSA was stored in air-tight containers for future use.

Adsorption studies

Adsorption experiments were performed for a single component using batch adsorption methods on a thermostatic shaker (SHA-C, Jiangsu, China). A known weight of XSA (50 mg) was dispersed into 50 mL of the aqueous Fe(III), Co(II), and Ni(II) solutions placed in a series of 100 mL capped Erlenmeyer flasks. The suspension was stirred at a uniform speed of 150 rpm for a given time while maintaining a constant temperature. The solution pH values were adjusted to a constant value using 1 M HCl and NaOH solutions. After reaching adsorption equilibrium, the mixtures were centrifuged at 6,000 rpm for 10 min to separate the activated carbon from the solution. The concentrations of each metal ion remaining in the filtrates were determined using a UV-visible spectrophotometer (TU-1901, Beijing, China) (Chen *et al.* 2003). The influential factors, such as the initial heavy metal concentration (550–800 mg/L), pH value (2.0–6.5), adsorption temperature (20–70 °C), and contact time (20–120 min), were varied to optimize the adsorption conditions. Each determination was conducted three times, and the results are provided as average values. In addition, a fourth flask containing only the metal ion solution (no activated carbon) was used as the control, and the reproducibility of the experimental results was within 3%. Adsorption kinetics and isotherm studies were carried out using various metal concentrations and different contact times and adsorption temperatures. The amounts of metal ions absorbed at equilibrium per unit mass of XSA were evaluated according to Nagpal *et al.* (2011) as follows:

$$q_{t,1} = \frac{(C_0 - C_{t,1})V_1}{m_1} \quad (1)$$

where $q_{t,1}$ (mg/g) is the adsorption capacity of the heavy metal ions at time t (min); C_0 and $C_{t,1}$ (mol/L) refer to the initial metal ion concentrations and the final concentration at time t (min); V_1 (mL) refers to the volumes of the Fe(III), Co(II), and Ni(II) solutions, respectively; and m_1 (g) is the mass of XSA. To calculate $q_{t,1}$, it was assumed that no loss of metal ions occurred during the experimental procedures.

Desorption and regeneration studies

HNO_3 was used as the elution reagent, and the desorption experiments were conducted as follows. The metal-loaded XSA (50 mg) was accurately weighed and dissolved in HNO_3 solutions (50 mL) with different concentrations. The mixture was placed in an ultrasonic cleaning machine (KS-300EI, Ninbo, China). After desorption equilibrium was reached, the suspension was centrifuged (6,000 rpm) and the concentration of the desorbed metal ions was determined. Similarly, desorption experiments were repeated three times, and the reducibility of the experimental results was within ±3%. The desorption capacity of XSA was calculated using the following equation (Zhang & Wang 2010; Kamble *et al.* 2011):

$$q_{t,2} = \frac{C_{t,2}V_2}{m_2} \quad (2)$$

where $q_{t,2}$ (mg/g) is the amount at desorption time t (min); $C_{t,2}$ (mol/L) is the concentration of each metal ion in solution at time t (min); V_2 (mL) is the volume of the HNO_3 solution; and m_2 (g) is the final mass of the XSA after the metal ions were released.

To investigate the reusability of the XSA, repeated adsorption/desorption experiments were performed. After the first batch adsorption experiment, the activated carbon was washed with re-deionized distilled water to remove the remaining acid and then dried in a vacuum (DZF-6210, Shanghai, China) at 70 °C before performing the next adsorption experiments. The regenerated XSA was used in five consecutive cycles under identical conditions.

Characterization

The BET specific surface area, pore structure and pore size of XSBH and XSA were measured using nitrogen adsorption/desorption isotherms at 196 °C (Micromeritics ASAP 2020, USA). Morphological changes and surface analysis of the samples were recorded using SEM-EDX (Hitachi S-4800). Chemical characterization of the functional

groups was detected using an FTIR spectrophotometer (Thermo Nicolet, NEXUS, TM) with a scanning range of 4,000–400 cm^{-1}.

RESULTS AND DISCUSSION

Characterization of the activated carbon

The surface morphological features of XSA determined using SEM is illustrated in Figure 1. As shown in Figure 1, XSA had uniform and organized pores, shapes, cracks, grains, and two main types of pore structures, large open pores and small closed pores. The external surface of the chemically activated XSA was full of cavities, which potentially provided a large number of activated sites and improved the ability of the XSA to adsorb heavy metals.

The surface area and elemental analysis are the important properties of activated carbon. Table 1 provides a comparison of the surface porosity structure parameters and elemental analysis of XSA by using H_3PO_4, $ZnCl_2$ and KOH as chemical activation agent, obtained from the N_2 adsorption/desorption isotherm and EDX. From the data in Table 1, it can be observed that the BET surface area, Langmuir surface area and total pore volume of XSA using H_3PO_4 as activation agent were relatively high (compared with $ZnCl_2$ and KOH) and reached maximum values of 688.62 m^2/g, 1,132 m^2/g and 0.377 cm^3/g, respectively. Meanwhile, the results represented an average pore diameter of 2.20 nm, implying that most of the mesoporous structures developed during the chemical activation process (Kırbıyık *et al.* 2016). Additionally, it also can be seen from the Table 1 that carbon and oxygen are the main components of XSA because carboxyl and hydroxyl groups are potential functional groups for heavy metals. The results indicated that XSA has higher carbon content and oxygen content during H_3PO_4 activation treatment (Abdolali *et al.* 2015). These signals were consistent with the FTIR spectral data. Based on the above-mentioned discussion, XSA can allow the formation of adequate activated sites and functional groups for chelation and complexation with heavy metals.

The values of adsorption capacity by other activated carbons from various materials in literature are presented in Table 2 for comparison. It is clear from this table that the adsorption capacity of XSA for Fe(III), Co(II), and Ni(II) is much higher than with other activated carbons.

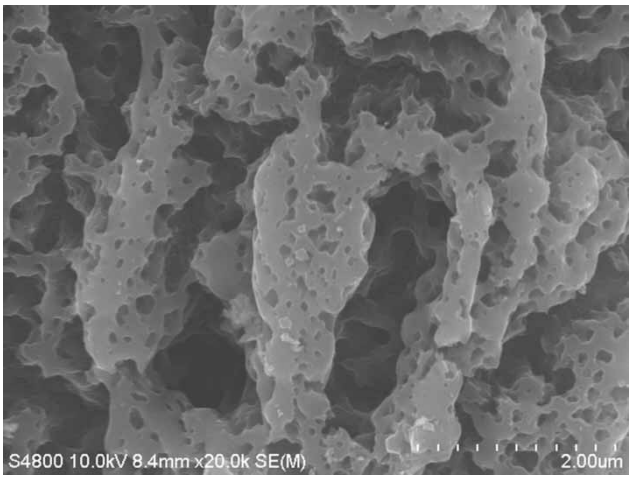

Figure 1 | Scanning electron microphotograph of XSA.

Adsorption studies

Effects of initial metal concentrations

The initial metal concentration is a significant factor for adsorption processes. To estimate the adsorption capacity of XSA, a batch of adsorption experiments was conducted by varying the initial metal concentrations. Figure 2(a) shows the relationships between the adsorption capacity and the initial concentrations of different metals. The adsorption capacity increased from 199.96 mg/g to 224.10 mg/g for Fe(III), from 65.24 mg/g to 126.05 mg/g for Co(II), and from 75.23 mg/g to 187.96 mg/g for Ni(II)

Table 1 | Porosity structure parameters and elemental analysis of XSA

Activate carbon	BET surface area (m^2/g)	Langmuir surface area (m^2/g)	Total pore volume (cm^3/g)	Average pore size (nm)	Carbon (at. %)	Oxygen (at. %)	Hydrogen (at. %)	C/O (%)	C/H (%)
XSA (H_3PO_4)	688.62	1,132.08	0.377	2.20	80.29	12.92	1.15	6.21	69.82
XSA ($ZnCl_2$)	354.81	485.09	0.214	19.85	74.10	8.27	1.09	8.96	67.98
XSA (KOH)	404.30	697.20	0.095	26.47	71.36	7.45	1.38	9.58	51.71

Number of analyses: three.

Table 2 | Comparison of adsorption capacity for Fe(III), Co(II), and Ni(II) adsorption onto XSA and activated carbons from other raw materials

	Adsorption capacity (mg/g)			
Adsorbent	**Fe(III)**	**Co(II)**	**Ni(II)**	**Reference**
XSA	241.13	126.05	187.96	Present study
Pineapple peel activated carbon	–	–	64.30	Dotto *et al.* (2016)
Bio-char activated carbon	65.36	–	–	Kırbıyık *et al.* (2016)
Hazelnut shell activated carbon	–	13.88	–	Demirbas (2003)

with the initial metal concentration range of 560–800 mg/L. This result is ascribed to the fact that higher initial metal concentrations correspond to greater driving forces of the concentration gradient at the interface between the solid and liquid phases. The adsorption reactions on the surface of XSA mainly include electrostatic attraction, ion exchange, and chelation between metal ions and functional groups. As the initial metal concentration increases, the driving force improves to overcome the mass transfer resistance between the solid and liquid interface, and a rapid increase in the adsorption capacity is observed. Then, additional increases in the metal concentration result in no changes because the functional groups are nearly occupied and saturated by competing metals and because no activated sites are left on the surface for further adsorption (Shroff & Vaidya 2011).

When comparing the Fe(III), Co(II), and Ni(II) ions, the adsorption capacity of Fe(III) is maximum. This result may be explained by the following observations. (1) The ionic radii of the ions increase as follows: Fe(III) (60 pm) < Ni(II) (70 pm) < Co(II) (72 pm). Smaller ionic radii correspond to a greater affinity of the metal for the active sites.

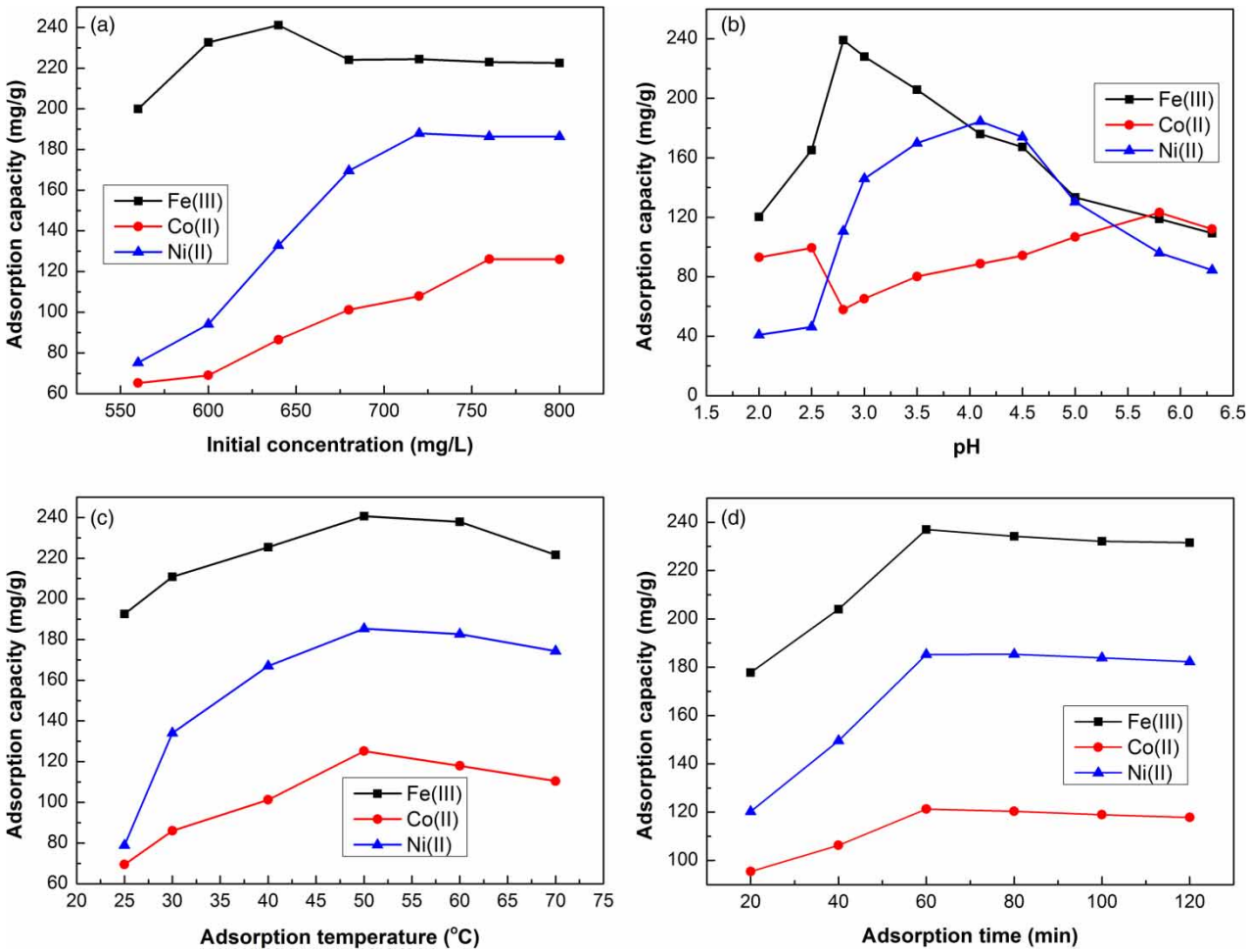

Figure 2 | Effects of the initial concentrations (a), pH (b), adsorption temperature (c) and adsorption time (d) on the adsorption capacities of Fe(III), Co(II), and Ni(II) ions by XSA.

(2) Chelation may produce coordination compounds between metal ions and the functional groups $-COO^-$ and $-OH^-$ on the surface of XSA. The oxidation number of Fe(III) is +3, with a common coordination number of 6, and the oxidation number of Ni(II) and Co(II) is +2, with a common coordination number of 4. Larger coordination numbers result in a greater adsorption capacity. In addition, the octahedral complex (d^2sp^3) of Fe(III) is packed and more stable than the tetrahedron complexes (dsp^2) of Co(II) and Ni(II) ions. (3) The electronegativities are 1.96 for Fe(III), 1.91 for Ni(II), and 1.88 for Co(II). It is well known that higher electronegativity corresponds to greater element reactivity. Thus, the reactivity of the metals with XSA decreased as follows: Fe(III) > Ni(II) > Co(II). (4) According to the periodic table, the arrangement of single electrons in the 3d orbitals of Fe(III), Co(II) and Ni(II) are $3d^5$, $3d^7$, and $3d^8$, respectively. Thus, the outer valence electrons of Fe(III) are arranged as $3d^5$, which is a semi-stable state, and the valence electrons of Co(II) are arranged as $3d^7$, which is less stable, and can lose two electrons, and the valence electrons of Ni(II) are arranged as $3d^8$, which is the least stable, and can lose three electrons. Thus, the metallic properties of XSA for Fe(III), Ni(II), and Co(II) adsorption gradually decrease. Based on the above discussion, ion exchange, electrostatic attraction and chelation are the most beneficial for Fe(III) adsorption on XSA, followed by Ni(II) and Co(II). In summary, Fe(III) was present at a minimum initial concentration of 640 mg/L and had a maximum adsorption capacity of 241.13 mg/g.

Effects of pH

The pH plays an important role in controlling the adsorption of heavy metal ions from aqueous solutions because it directly impacts the abilities of the metal to compete with H^+ and functional groups on the surface of the adsorbent (Zarandi *et al.* 2016). Thus, the pH was examined and was observed to vary from 2.0 to 6.3. The effects of pH on Fe(III), Co(II), and Ni(II) adsorption to XSA are shown in Figure 2(b). As shown in Figure 2(b), the adsorption increased from 120.21 mg/g to 239.12 mg/g for Fe(III), 93.01 mg/g to 184.42 mg/g for Co(II), and 40.85 mg/g to 123.16 mg/g for Ni(II) as the pH increased from 2.0 to 5.8, respectively. At higher pH values, adsorption of Fe(III), Co(II), and Ni(II) ions decreased to different degrees.

The adsorption of Fe(III), Co(II), and Ni(II) was very low at pH 2.0, which may be attributed to the fact that the high concentration of H^+ in the highly acidic solution competes with the metal ions for the functional sites that have been protonated on the surface of XSA, resulting in electrostatic repulsion and the suppression of metal adsorption. For Fe(III) ions, functional groups such as carboxyl and hydroxyl groups begin to deprotonate by releasing H^+ ions when the pH increases (2.0–2.8), and more negatively charged sites become available, which facilitates Fe(III) uptake. Maximum adsorption occurs at pH 2.8. At pH values higher than 2.8, hydrolysis and polymerization greatly increase, leading to the formation of gelatinous $Fe(OH)_3$ sediment; therefore, the adsorption of Fe(III) decreases. For Co(II) and Ni(II), the optimal pH values are 5.8 and 4.1, respectively. The surface of XSA is more negatively charged and more easily attracts positively charged metallic cations when the pH is between 2.0 and 5.8 for Co(II) and between 2.0 and 4.1 for Ni(II). Furthermore, at higher pH values, Co(II) (pH > 5.8) and Ni(II) (pH > 4.1) can be hydrolysed, generating the amphoteric hydrolysis products $Co(OH)_2$ and $Ni(OH)_2$, and K^o_{sp} $[Co(OH)_2]$ $1.60 \times 10^{-15} > K^o_{sp}$ $[Ni(OH)_2]$ 6.48×10^{-16}, which indicates that the solubility of these ions increased and the adsorption capacity decreased. Thus, the adsorption capacity is greater for Ni(II) than for Co(II). In summary, the adsorption capacities of the ions decrease as follows: Fe(III) > Ni(II) > Co(II).

Effects of temperature

The influences of temperature on adsorption should be investigated when considering practical applications. A correlation between the adsorption temperature and adsorption capacity was observed from 25 °C to 70 °C and is illustrated in Figure 2(c). As observed in the figure, the adsorption capacities of Fe(III), Co(II), and Ni(II) all increased and reached maximum adsorption capacities of 192.56 mg/g to 240.61 mg/g for Fe(III), 69.43 mg/g to 125.15 mg/g for Co(II), and 78.91 mg/g to 185.32 mg/g for Ni(II) as the temperature increased from 25 °C to 50 °C, which indicated that higher temperatures are conducive to the adsorption of metal ions on XSA. This result potentially occurs because physical adsorption mainly takes place when the temperature is near room temperature, resulting in a certain amount of adsorption. When the temperature increased, chemisorption was dominant, which was potentially the result of increasing the kinetic energy in the solution, which increased the probability of collisions between the metals and activated sites. In addition, increasing temperatures may produce a swelling effect within the mesoporous structure, which facilitates the uptake of metals. The general upward tendency also indicates that the adsorption process

is endothermic and that net heat adsorption occurs. However, a slight decrease in the adsorption capacity at higher temperatures (>50 °C) may occur because the chemical adsorption process is exothermic, spontaneous and entropy reducing; thus, as the temperature increases, the adsorption capacity would decrease. In addition, at high temperatures (>50 °C), the bonds between the metals and functional groups may be destroyed and desorption is favoured. Then, additional studies were carried out using an adsorption temperature of 50 °C for all of the iron group ions. Meanwhile, the same decreasing trend in adsorption capacity of Fe(III) > Ni(II) > Co(II) was observed.

Effects of adsorption time

It is important to determine the effects of the amount of time required to reach the adsorption equilibrium when conducting a batch of experiments. Figure 2(d) shows the influences of adsorption time on the adsorption of metal ions by XSA. As shown in Figure 2(d), the adsorption capacities of the Fe(III), Co(II) and Ni(II) ions increased rapidly from 177.81 mg/g to 236.98 mg/g for Fe(III), from 95.43 mg/g to 121.27 mg/g for Co(II), and from 120.19 mg/g to 185.29 mg/g for Ni(II), respectively, as the adsorption time increased from 20 min to 60 min. Next, the adsorption equilibrium reached a plateau for a prolonged period. This result could explain why metals were adsorbed by diffusion into the microporous structure and high vacancy active sites on the surface of XSA. In addition, coordination and chelation complexes were generated between the metals and functional groups, resulting in a sharp adsorption equilibrium. Thereafter, no further adsorption occurred with prolonged adsorption until 120 min, which may be attributed to the saturation of the functional groups and activated sites on the surface of XSA. Consequently, the optimal adsorption time is 60 min in this study for the removal of the iron group ions by XSA. Similar results of adsorption capacity, with a descending order of Fe(III) > Ni(II) > Co(II), were obtained.

Adsorption kinetics

Predictions of adsorption rates provide important information regarding adsorption mechanisms. To evaluate the kinetics of Fe(III), Co(II), and Ni(II) adsorption onto XSA, the experimental data at various adsorption times corresponding to the changes in adsorption capacity were fit using pseudo-first order, pseudo-second order, intraparticle diffusion and Elovich models (Kilic *et al.* 2011), which are described as Equations (3)–(6). During the full-scale batch adsorption process, the following optimal operating conditions were selected: (i) an initial concentration of 640 mg/L and a pH of 2.8 for Fe(III); (ii) an initial concentration of 760 mg/L and pH 5.8 for Co(II); and (iii) an initial concentration of 720 mg/L and pH 4.1 for Ni(II) at 50 °C, 150 rpm and using 50 mg of XSA.

$$\ln (q_e - q_t) = \ln q_e - k_1 t \tag{3}$$

$$\frac{t}{q_t} = \frac{t}{q_e} + \frac{1}{k_2 q_e^2} \tag{4}$$

$$q_t = k_i t^{0.5} \tag{5}$$

$$q_t = \frac{1}{\beta}\ln (\alpha\beta) + \frac{1}{\beta}\ln t \tag{6}$$

where q_e and q_t are the amounts of heavy metal ions adsorbed (mg/g) at equilibrium and at time t (min), respectively; k_1 (min^{-1}) is the pseudo-first-order rate constant; k_2 [g·(mg/min)$^{-1}$] is the rate constant of the pseudo-second-order adsorption kinetic equation; k_i [mg/(g $\text{min}^{0.5}$)] is an intraparticle diffusion rate constant; α [mg/(g min)] is an initial adsorption rate; and β (g/mg) is related to the surface coverage and activation energy for chemisorption.

The fits of these four models were checked by each linear plot of ln (q_e–q_t) versus t (pseudo-first-order model), (t/q_t) versus t (pseudo-second-order model), q_t versus $t^{0.5}$ (intraparticle diffusion), and q_t versus ln$t$ (Elovich model), respectively. The R^2 and constant values for the four adsorption kinetic models were calculated and are given in Table 3. According to the calculated kinetic model parameters in Table 3 and from comparing the experimental equilibrium adsorption capacity, it was found that the values provided by the pseudo-second-order model were more similar to the estimated equilibrium adsorption capacity than those provided by the pseudo-first-order, intraparticle diffusion and Elovich models. Also, it could be observed that the R^2 value of the pseudo-second-order kinetic model was close to 1.0 (R^2 Fe(III), 0.9952, R^2 Co(II), 0.9957; R^2 Ni(II), 0.9886). These results suggested that the pseudo-second-order model better described the adsorption kinetic processes of Fe(III), Co(II) and Ni(II) onto XSA. Therefore, it is obvious that chemical adsorption should be the rate limiting step of the adsorption of iron group ions onto the prepared activated carbon XSA.

Table 3 | R^2 and constant values for the different adsorption kinetics models of Fe(III), Co(II) and Ni(II)

Metal	Parameters	Pseudo-first-order		Pseudo-second-order		Intraparticle diffusion		Elovich model	
Fe(III)	R^2	0.9419		0.9952		0.6637		0.7768	
	Constants	k_1	0.03459 min^{-1}	k_2	1.1295×10^{-4} g·(mg/min)$^{-1}$	k_i	16.648 mg/(g $min^{0.5}$)	α	17.1030 mg/(g min)
		q_e	187.64 mg/g	q_e	239.47 mg/g			β	0.01644 g/mg
Co(II)	R^2	0.8407		0.9957		0.6263		0.7428	
	Constants	k_1	0.002859 min^{-1}	k_2	0.9648×10^{-3} g·(mg/min)$^{-1}$	k_i	1.4292 mg/(g $min^{0.5}$)	α	84.3347 mg/(g min)
		q_e	162.6953 mg/g	q_e	122.51 mg/g			β	0.01288 g/mg
Ni(II)	R^2	0.8650		0.9886		0.7088		0.8157	
	Constants	k_1	0.0246 min^{-1}	k_2	1.2791×10^{-3} g·(mg/min)$^{-1}$	k_i	1.8161 mg/(g $min^{0.5}$)	α	1.95885×10^{5} mg/(g min)
		q_e	110.5062 mg/g	q_e	179.47 mg/g			β	01410 g/mg

Adsorption isotherm

Adsorption isotherms define the characteristics of the adsorption process and are very important for describing how metals interacted with adsorbents to guide useful application in wastewater treatment. The Langmuir, Freundlich, Temkin and Dubinin–Radushkevich models were applied to fit the adsorption equilibrium data obtained from the batch adsorption systems, which are expressed as Equations (7)–(11) (Roy *et al.* 2013).

$$\frac{C_e}{q_e}=\frac{1}{K_L q_{\max}}+\frac{C_e}{q_{\max}} \tag{7}$$

$$\ln q_e=\ln K_f+\frac{1}{n}\ln C_e \tag{8}$$

$$q_e=\frac{RT}{b_t}\ln \alpha_t+\frac{RT}{b_t}\ln C_e \tag{9}$$

$$\ln q_e=\ln q_{\max}-B\varepsilon^2 \tag{10}$$

$$\varepsilon=RT\ln\left(1+\frac{1}{C_e}\right) \tag{11}$$

where K_L (L/mg) is the Langmuir constant related to the adsorption capacity; $q_{\max}$ (mg/g) is the monolayer saturation adsorption capacity; $1/n$ is the value used to indicate the heterogeneity of the interface; K_f is the Freundlich constant; C_e (mg/L) is the concentration of metal ions at equilibrium; q_e (mg/g) is the adsorption capacity at equilibrium; R is the ideal gas constant (8.314 J/(mol·K)); T (K) is the absolute temperature of the adsorption process; α_t (L/g) and b_t (J/mol) are Temkin isotherm constants; B is a constant; and ϵ is the Polanyi potential, which can be calculated using Equation (11).

Comparisons of these isotherm models for the adsorption of the iron group ions onto XSA was performed by comparing each linear plot of C_e/q_e versus C_e (Langmuir isotherm model), $\ln q_e$ versus $\ln C_e$ (Freundlich isotherm model), q_e versus $\ln C_e$ (Temkin isotherm model), and $\ln q_e$ versus ε^2 (Dubinin–Radushkevich isotherm model). The calculated constants are listed in Table 4. From Table 4, it is clear that

Table 4 | R^2 and constant values for the different adsorption isotherm models of Fe(III), Co(II) and Ni(II)

Metal	Parameters	Langmuir		Freundlich		Temkin		Dubinin–Radushkevich	
Fe(III)	R^2		0.9914		0.9375		0.5353		0.6229
	Constants	K_L	0.0275 L/mg	K_f	99.15 L/g	b_t	27.06 J/mol	B	2.615×10^{-7} mol^2/J^2
		R_L	0.0538						
		$q_{\max}$	241.13 mg/g	$1/n$	0.472	a_t	1.854×10^{9} L/g	$q_{\max}$	143.29 g/mg
Co(II)	R^2		0.9846		0.9194		0.8896		0.9034
	Constants	K_L	0.0057 L/mg	K_f	101.07 L/g	b_t	74.33 J/mol	B	1.260×10^{-7} mol^2/J^2
		R_L	0.188						
		$q_{\max}$	126.05 mg/g	$1/n$	0.116	a_t	6.170×10^{10} L/g	$q_{\max}$	64.32 g/mg
Ni(II)	R^2		0.9957		0.8381		0.8247		0.9004
	Constants	K_L	0.0173 L/mg	K_f	89.23 L/g	b_t	80.29 J/mol	B	9.863×10^{-7} mol^2/J^2
		R_L	0.0743						
		$q_{\max}$	187.96 mg/g	$1/n$	0.689	a_t	7.059×10^{9} L/g	$q_{\max}$	167.88 g/mg

the Langmuir model provides the best fit relative to the other models, with maximum monolayer adsorption capacities of 249.56 mg/g for Fe(III), 126.05 mg/g for Co(II), and 187.96 mg/g for Ni(II) and R^2 values of 0.9914, 0.9846, and 0.9957, respectively. Interestingly, the R^2 values of the four isotherm models decreased in the following order: Langmuir > Freundlich > Dubinin–Radushkevich > Temkin for Fe(III); Langmuir > Freundlich > Dubinin–Radushkevich > Temkin for Co(II); and Langmuir > Dubinin–Radushkevich > Temkin > Freundlich for Ni(II). It is understood that the Langmuir model corresponded to a dominant electrostatic attraction, ion exchange, and chelation mechanism, while the order revealed that the adsorption process involved physical adsorption and complexation at the interface and the outer heterogeneous surface of XSA.

The essential characteristics of the Langmuir isotherm can be represented according to a dimensionless equilibrium parameter (R_L) based on the following equation:

$$R_L = \frac{1}{1 + K_L C_0} \tag{12}$$

where K_L (L/mg) is the Langmuir adsorption constant and C_0 is the optimal concentration of Fe(III), Co(II) and Ni(II) ions. The value of R_L indicates the nature of the isotherm as unfavourable ($R_L > 1$), linear ($R_L = 1$), favourable ($0 < R_L < 1$), or irreversible ($R_L = 0$).

Table 4 shows the calculated R_L values, which were 0.0538 for Fe(III), 0.188 for Co(II) and 0.0743 for Ni(II), respectively. The results implied that XSA was favourable for the adsorption of iron group ions under the adsorption conditions employed in the current work.

Desorption and regeneration studies

Effects of HNO_3 concentration

The desorption of the iron group ions adsorbed on the XSA activated carbon was examined using an aqueous solution of HNO_3. The effects of different HNO_3 concentrations on the desorption capacity of metal-loaded XSA are shown in Figure 3(a). The desorption capacity of XSA increased and then remained nearly constant as the HNO_3 concentration

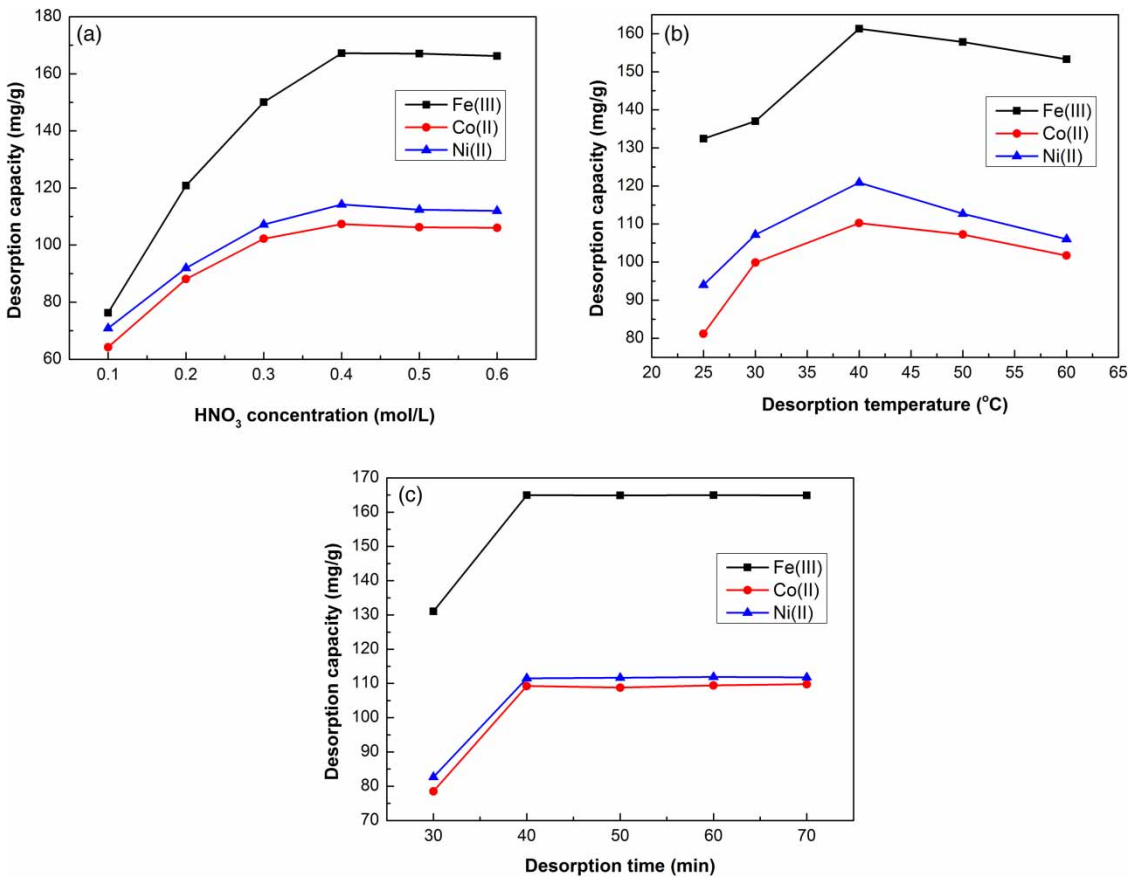

Figure 3 | Effects of the HNO_3 concentration (a), desorption temperature (b), and desorption time (c) on the desorption capacities of Fe(III), Co(II), and Ni(II) ions by XSA.

increased. Under acidic conditions, it seemed like the XSA surface was protonated by H^+ ions to allow for the desorption of positively charged metal ions from the surface of the XSA. Based on the influences of HNO_3 on the removal of the iron group ions, electrostatic interactions played an important role in Fe(III), Co(II), and Ni(II) adsorption processes, and the use of the HNO_3 solution for desorption was effective because ion exchange reactions occurred between the active sites on the XSA and the H^+ and metal ions, which further substantiated the influences of solution pH on adsorption. This observation was very similar to previously reported results (Lalhruaitluanga *et al.* 2010). The maximum amount of XSA desorption reached 167.23 mg/g for Fe(III), 107.34 mg/g for Co(II), and 114.22 mg/g for Ni(II) when the HNO_3 concentration was 0.4 mol/L.

Effect of desorption temperature

The effects of different desorption temperatures on the desorption capacity of metal-loaded XSA are shown in Figure 3(b). The amount of desorption increased before slightly decreasing with increasing temperature. This fluctuation in desorption could be attributed to the fact that increasing temperature may improve the adsorption efficiency of the active sites and because H^+ and the iron group ions can compete with each other for activate sites on the surface, increasing the desorption capacity when the temperature increases. In addition, the adsorption efficiency of the active sites may be weakened at a temperature above 40 °C, thus producing a detrimental effect on desorption (Bas *et al.* 2014), which further substantiated the results of adsorption temperature. The desorption capacity decreased in the following order: Fe(III) > Ni(II) > Co(II).

Effects of sonication time

The effects of different desorption sonication times on the metal-loaded XSA are shown in Figure 3(c). The desorption capacity increased during the first stage, and then no further increase occurred after desorption equilibrium and with increasing sonication time. This phenomenon corresponds to the ultrasound rules of producing holes. After a certain ultrasound reaction time, the number of holes in the solution reached saturation, the high temperature generated ultrasonic cavitation, and the high pressure increased the adsorbate energy, which was favourable for desorption (Mata *et al.* 2010). The desorption capacity still decreased from Fe(III) > Ni(II) > Co(II) at an optimum sonication time of 60 min.

Recycling and reusability

Recovering and reusing an adsorbent would decrease processing costs and is very important for technical applications. The reusability of XSA was tested by performing five consecutive adsorption/desorption processes for each metal ion. All of the adsorption and desorption capacities of the iron group ions in the consecutive cycles are tabulated in Table 5. The data showed that XSA could be recycled up to three times for Co(II) and up to four times for Fe(III) and Ni(II) ions with very little loss of efficiency. Up to the 3rd–4th cycles, it was clear that the capacities of adsorption and desorption had excellent performance, indicating that XSA could be an economically feasible method for the removal of iron group ions from wastewater treatment.

Adsorption mechanism

To elucidate the adsorption mechanisms and validate the hypothesis of the interactions between the metal and adsorbent, FTIR analysis was utilized to examine the characteristic chemical structures of purified XSA, metal-loaded XSA and the desorption of Fe(III) samples within the wavenumber range of 400–4,000 cm^{-1}. As shown in Figure 4, several absorbance bands from the FTIR spectrum of XSA (Figure 4(a)) were found, such as the –OH stretching vibration mode of the hydroxyl functional groups (3,440 cm^{-1}), the C-H vibration

Table 5 | Adsorption/desorption capacities for Fe(III), Co(II) and Ni(II) ions on XSA after five consecutive cycles

Metal	Recycle times	1st	2nd	3rd	4th	5th
Fe(III)	Adsorption capacity (mg/g)	241.13	220.35	217.40	196.33	102.17
	Desorption capacity (mg/g)	167.23	149.61	135.06	120.88	64.20
Co(II)	Adsorption capacity (mg/g)	126.05	122.14	101.37	74.20	57.18
	Desorption capacity (mg/g)	110.25	99.26	86.46	59.23	47.19
Ni(II)	Adsorption capacity (mg/g)	187.96	179.64	160.30	152.87	85.36
	Desorption capacity (mg/g)	120.89	112.40	101.52	91.27	49.88

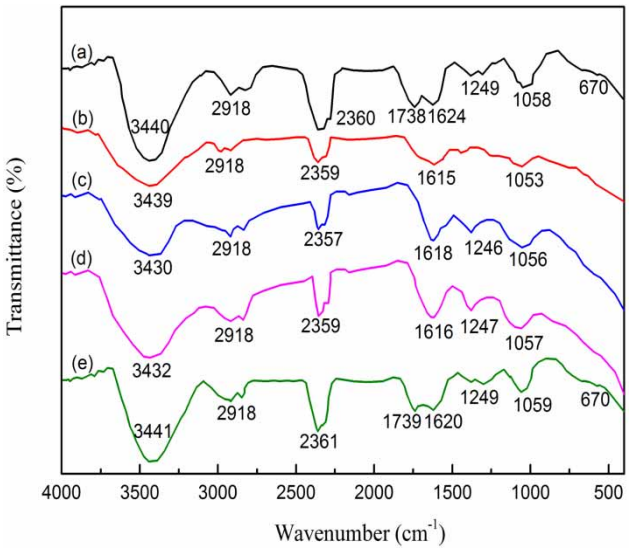

Figure 4 | FTIR spectra of purified XSA (a), Fe(III)-loaded XSA (b), Ni(II)-loaded XSA (c), Co(II)-loaded XSA (d), and XSA after desorption of Fe(III) (e).

of methyl groups (2,918 cm^{-1}), the C ≡ C vibration of alkyne groups (2,360 cm^{-1}), the –C = O stretching vibration of carboxyl groups (1,738 cm^{-1}), the C = O of carbonyl (e.g., ketone) and carboxylate ion (COO^-) groups (1,624 cm^{-1}), the C-H stretching of alcoholic groups (1,249 cm^{-1}), and the C-O of carboxylic acid (1,058 cm^{-1}) and O-H vibration groups (670 cm^{-1}).

The asymmetrical stretching vibration at 3,440 cm^{-1} (Figure 4(a)) decreased and shifted to lower wavenumbers of 3,439, 3,430 and 3,432 cm^{-1} after the adsorption of Fe(III), Ni(II) and Co(II) (Figure 4(b)–4(d)), respectively, especially for Fe(III) ions. The spectra of XSA after Fe(III) desorption were chosen as a model for assessing the differences due to the interactions between metal ions and functional groups on the surface of XSA (Figure 4(e)). The changes in –OH adsorption showed that the degree of hydroxyl polymerization varied from multimer to monopolymer in the XSA by binding Fe(III), Ni(II) and Co(II) ions (Figure 4(b)–4(d)), and Fe(III) had a higher binding capacity for XSA, and the asymmetrical stretching vibration was restored to 3,441 cm^{-1} after Fe(III) desorption (Figure 4(e)). Interestingly, the characteristic adsorption band at 1,738 cm^{-1} (Figure 4(a)), which corresponds to the asymmetric stretching vibration of the C = O bond in carboxylic acids, was diminished after adsorption of Fe(III), Ni(II) and Co(II) (Figure 4(b)–4(d)) and slightly weakened after desorption of Fe(III) at a lower wavenumber of 1,729 cm^{-1} (Figure 4(e)). The changes in the peak at 1,624 cm^{-1} (Figure 4(a)) correspond to the carbonyl and carboxylate groups that were reduced after adsorption of the iron group ions at 1,615, 1,618, and 1,617 cm^{-1} (Figure 4(b)–4(d)), and were slightly regained after desorption of Fe(III) at a lower wavenumber of 1,620 cm^{-1} (Figure 4(e)). The peak at 1,058 cm^{-1} (Figure 4(a)) was reduced and moved to $1{,}053^{-1}$ after adsorption for Fe(III) (Figure 4(b)), 1,056 cm^{-1} for Ni(II) (Figure 4(c)), and 1,057 cm^{-1} for Co(II) (Figure 4(d)). The adsorption effect for Fe(III) ions was typically the highest, which indicated that the combined ability of Fe(III)-XSA was higher than that of Co(II) and Ni(II). Then, the peak slightly decreased at 1,059 cm^{-1} after Fe(III) desorption (Figure 4(e)), which corresponded with the results of the adsorption experiments. From these observations, it was tentatively concluded that the major adsorption sites on the surface of XSA for metal binding are the hydroxyl, carboxyl and carboxyl functional groups and that other groups (methyl, C ≡ C, methylene) hardly changed. In addition, slight changes were observed in the FTIR spectra of Fe(III) desorption, and the spectra were basically restored to their original shape. In conclusion, the coordination of Fe(III), Co(II) and Ni(II) ions with the presented functional groups and the chemical adsorption are predominant in the adsorption process of the iron group ions. Additionally, the basic structures and properties of XSA remained relatively stable during the process of metal adsorption and desorption, indicating that XSA is a good renewable adsorbent for wastewater treatment.

The most plausible explanations for the descending order of adsorption of Fe(III) > Ni(II) > Co(II) is that the ionic radius, the oxidation number, electronegativity, and the arrangement of the valence single electrons influenced the adsorption of the iron group ions by XSA, with a smaller ionic radius, higher oxidation number, greater electronegativity, and more stable outer electron arrangement resulting in preferential absorption.

The EDX is an analytical technique used for elemental analysis. Owing to good effects of adsorption and desorption capacity in the experimental tests, we used Fe(III) ion as an example to investigate the adsorption mechanism. EDX analysis of XSA was performed to confirm existence of Fe(III) on Fe(III)-loaded XSA. EDX spectra of purified XSA, Fe(III)-loaded XSA and recovered XSA are shown in Figure 5. In the EDX spectrum, two new peaks of Fe(III) were found in Fe(III)-loaded XSA, confirming the presence of Fe(III) ions (Figure 5(b)). After desorption, content of Fe(III) was decreased (Figure 5(c)).

CONCLUSION

In this work, a prepared XSA was tested for removing Fe(III), Co(II) and Ni(II) ions from aqueous solution. The

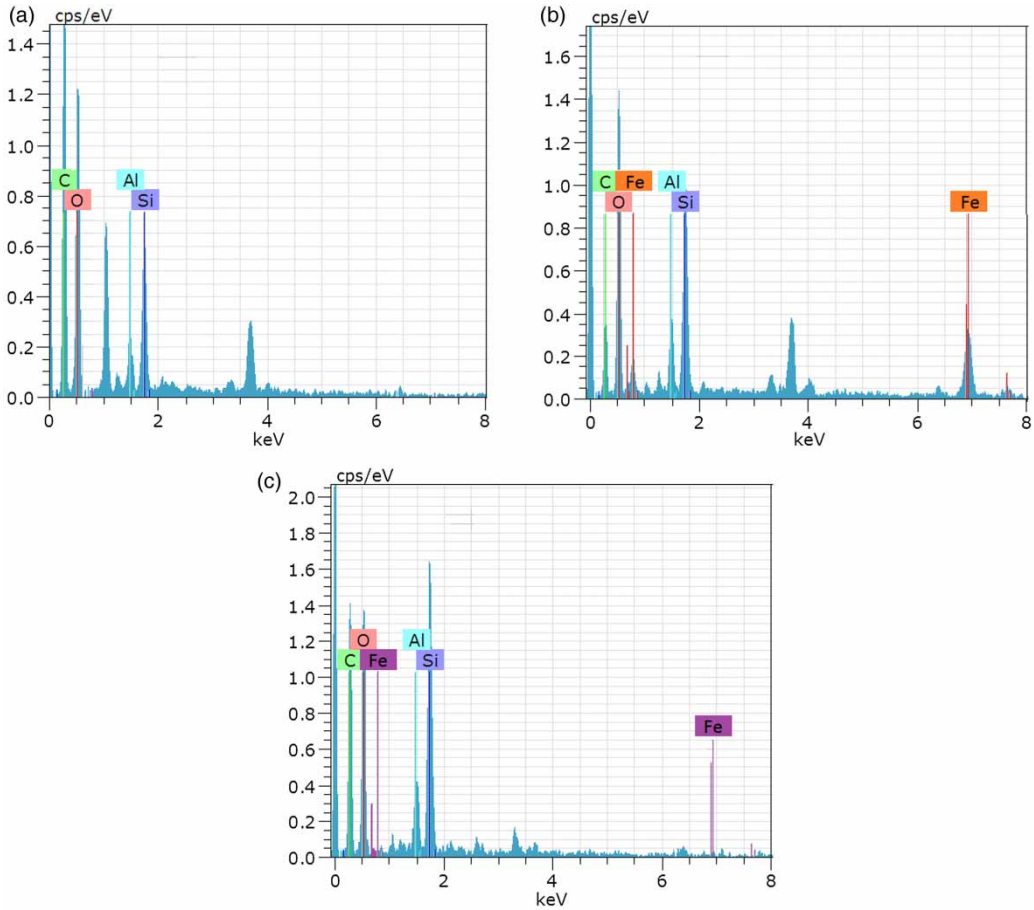

Figure 5 | EDX spectra for purified XSA (a), Fe(III)-loaded XSA (b) and XSA after desorption of Fe(III) (c).

maximum adsorption capacities were 241.13 mg/g for Fe(III), 126.05 mg/g for Co(II), and 187.96 mg/g for Ni(II), respectively. The adsorption kinetics and isotherm showed that the adsorption processes were described best by the pseudo-second-order and Langmuir models. Desorption and regeneration experiments revealed that HNO_3 was able to elute 167.23 mg/g of Fe(III), 107.34 mg/g of Co(II), and 114.22 mg/g of Ni(II). The FTIR and EDX spectra suggested the adsorption was a chemical adsorption process. Also, the ability of the metals to bind with XSA decreased in the following order: Fe(III) > Ni(II) > Co(II).

ACKNOWLEDGEMENTS

Authors Xiaotao Zhang and Yinan Hao contributed equally to this paper. We are grateful for financial support from the National Natural Science Foundation of PR China (No. 21467021) and the International Science & Technology Cooperation Program of China 2013DFA32000).

REFERENCES

Abdolali, A., Ngo, H. H., Guo, W., Zhou, J. L., Du, B., Wei, Q., Wang, X. C. & Nguyen, P. D. 2015 Characterization of a multi-metal binding biosorbent: chemical modification and desorption studies. *Bioresource Technology* **193**, 477–487. DOI: 10.1016/j.biortech.2015.06.123.

Azevedo, D. C. S., Araújo, J. C. S., Bastos-Neto, M., Torres, A. E. B., Jaguaribe, E. F. & Cavalcante, C. L. 2007 Microporous activated carbon prepared from coconut shells using chemical activation with zinc chloride. *Microporous & Mesoporous Material* **100** (1–3), 361–364. DOI: 10.1016/j.micromeso.2006.11.024.

Bas, N., Yakar, A. & Bayramgil, N. P. 2014 Removal of cobalt ions from aqueous solutions by using poly(N,N-dimethylaminopropyl methacrylamide/itaconic acid) hydrogels. *Journal of Applied Polymer Science* **131** (7), 39569. DOI: 10.1002/app.39569.

Chen, W., Westerhoff, P., Leenheer, J. A. & Booksh, K. 2003 Fluorescence excitation-emission matrix regional integration to quantify spectra for dissolved organic matter. *Environmental Science & Technology* **37** (24), 5701–5710. DOI: 10.1021/es034354c.

Choi, G. G., Oh, S. J., Lee, S. J. & Kim, J. S. 2015 Production of bio-based phenolic resin and activated carbon from bio-oil and biochar derived from fast pyrolysis of palm kernel shells. *Bioresource Technology* **178**, 99–107. DOI: 10.1016/j.biortech.2014.08.053.

Daud, W. M. A. W. & Ali, W. S. W. 2004 Comparison on pore development of activated carbon produced from palm shell and coconut shell. *Bioresource Technology* **93** (1), 63–69. DOI: 10.1016/j.biortech.2003.09.015.

Demirbas, E. 2003 Adsorption of cobalt(II) ions from aqueous solution onto activated carbon prepared from hazelnut shells. *Adsorption Science & Technology* **21** (10), 951–963. DOI: 10.1260/02636170360744380.

Depci, T., Kul, A. R. & Önal, Y. 2012 Competitive adsorption of lead and zinc from aqueous solution on activated carbon prepared from Van apple pulp: study in single- and multi-solute systems. *Chemical Engineering Journal* **200–202** (34), 224–236. DOI: 10.1016/j.cej.2012.06.077.

Dotto, G. L., Meili, L., Abud, A. K. S., Tanabe, E. H., Bertuol, D. A. & Foletto, E. L. 2016 Comparison between Brazilian agro-wastes and activated carbon as adsorbents to remove Ni(II) from aqueous solutions. *Water Science & Technology* **73** (11), 2713–2721. DOI: 10.2166/wst.2016.095.

Güzel, F., Yakut, H. & Topal, G. 2008 Determination of kinetic and equilibrium parameters of the batch adsorption of Mn(II), Co(II), Ni(II) and Cu(II) from aqueous solution by black carrot (*Daucus carota* L.) residues. *Journal of Hazardous Materials* **153** (3), 1275–1287. DOI: doi:10.1016/j.jhazmat.2007.09.087.

Kamble, G. S., Ghare, A. A., Kolekar, S. S., Han, S. H. & Anuse, M. A. 2011 Development of a reliable analytical method for synergistic extractive spectrophotometric determination of cobalt(II) from alloys and nano composite samples by using chromogenic chelating ligand. *Spectrochimica Acta Part A: Molecular and Biomolecular Spectroscopy* **84** (1), 117–124. DOI: 10.1016/j.saa.2011.09.015.

Kilic, M., Apaydin-Varol, E. & Pütün, A. E. 2011 Adsorptive removal of phenol from aqueous solutions on activated carbon prepared from tobacco residues: equilibrium, kinetics and thermodynamics. *Journal of Hazardous Materials* **189** (1–2), 397–403. DOI: 10.1016/j.jhazmat.2011.02.051.

Kırbıyık, Ç., Pütün, A. E. & Pütün, E. 2016 Comparative studies on adsorptive removal of heavy metal ions by biosorbent, bio-char and activated carbon obtained from low cost agro-residue. *Water Science & Technology* **73** (2), 423–436. DOI: 10.2166/wst.2015.504.

Lalhruaitluanga, H., Kottapalli, J., Majeti, P. & Kadimpati, K. K. 2010 Lead(II) adsorption from aqueous solutions by raw and activated charcoals of *Melocanna baccifera* Roxburgh (bamboo)–a comparative study. *Journal of Hazardous Materials* **175** (1–3), 311–318. DOI: 10.1016/j.jhazmat.2009.10.005.

Mata, Y. N., Blázquez, M. L., Ballester, A., González, F. & Muñoz, J. A. 2010 Studies on sorption, desorption, regeneration and reuse of sugar-beet pectin gels for heavy metal removal. *Journal of Hazardous Materials* **178** (1–3), 243–248. DOI: 10.1016/j.jhazmat.2010.01.069.

Molina-Sabio, M. & Rodrigues-Reinoso, F. 2004 Role of chemical activation in the development of carbon porosity. *Colloids and Surfaces A: Physicochemical and Engineering Aspects* **241** (1), 15–25. DOI: 10.1016/j.colsurfa.2004.04.007.

Moreno-Barbosa, J. J., López-Velandia, C., Maldonado, A. P., Giraldo, L. & Moreno-Piraján, J. C. 2013 Removal of lead(II) and zinc(II) ions from aqueous solutions by adsorption onto activated carbon synthesized from watermelon shell and walnut shell. *Adsorption* **19** (2), 675–685. DOI: 10.1007/s10450-013-9491-x.

Nagpal, U. M. K., Bankar, A. V., Pawar, N. J., Kapadnis, B. P. & Zinjarde, S. S. 2011 Equilibrium and kinetic studies on biosorption of heavy metals by leaf powder of paper mulberry (*Broussonetia papyrifera*). *Water Air and Soil Pollution* **215** (1), 177–188. DOI: 10.1007/s11270-010-0468-z.

Oliveira, R. C., Hammer, P., Guibal, E., Taulemesse, J. M. & Garcia Jr, O. 2014 Characterization of metal-biomass interactions in the lanthanum(III) biosorption on *Sargassum* sp. using SEM/EDX, FTIR, and XPS: preliminary studies. *Chemical Engineering Journal* **239**, 381–391. DOI: 10.1016/j.cej.2013.11.042.

Roy, A., Adhikari, B. & Majumder, S. B. 2013 Equilibrium, kinetic, and thermodynamic studies of azo dye adsorption from aqueous solution by chemically modified lignocellulosic jute fiber. *Industrial & Engineering Chemistry Research* **52** (19), 6502–6512. DOI: 10.1021/ie400236s.

Shroff, K. A. & Vaidya, V. K. 2011 Kinetics and equilibrium studies on biosorption of nickel from aqueous solution by dead fungal biomass of *Mucor hiemalis*. *Chemical Engineering Journal* **171** (3), 1234–1245. DOI: 10.1016/j.cej.2011.05.034.

Tabrizi, N. S. & Zamani, S. 2016 Removal of Pb(II) from aqueous solutions by graphene oxide aerogels. *Water Science & Technology* **74** (1), 256–265. DOI: 10.2166/wst.2016.213.

Tang, S. X., Yao, C., Xie, R. Z., Jiang, W. J. & Jiang, Y. X. 2016 Preparation of activated carbon from corn cob and its adsorption behavior on Cr(VI) removal. *Water Science & Technology* **73** (11), 2654–2661. DOI: 10.2166/wst.2016.120.

Tao, H. C., Zhang, H. R., Li, J. B. & Ding, W. Y. 2015 Biomass based activated carbon obtained from sludge and sugarcane bagasse for removing lead ion from wastewater. *Bioresource Technology* **192**, 611–617. DOI: 10.1016/j.biortech.2015.06.006.

Zarandi, M. J. E., Sohrabi, M. R., Khosravi, M., Mansouriieh, N., Davallo, M. & Khosravan, A. 2016 Optimizing Cu(II) removal from aqueous solution by magnetic nanoparticles immobilized on activated carbon using Taguchi method. *Water Science & Technology* **74** (1), 38–47. DOI: 10.2166/wst.2016.152.

Zhang, J. P. & Wang, A. Q. 2010 Adsorption of Pb(II) from aqueous solution by chitosan-*g*-poly(acrylic acid)/attapulgite/sodium humate composite hydrogels. *Journal of Chemical & Engineering Data* **55** (7), 2379–2384. DOI: 10.1021/je900813z.

First received 28 July 2016; accepted in revised form 23 January 2017. Available online 6 February 2017